JOURNAL OF SOLID STATE CHEMISTRY 67, 225–234 (1987)

# Structural Prereactional Transformations in $Ca(OH)_2$

O. CHAIX-PLUCHERY,* J. PANNETIER, AND J. BOUILLOT

*Institut Laue-Langevin, 156X, 38042 Grenoble Cedex, France*

AND J. C. NIEPCE

*Laboratoire de Recherche sur la Réactivité des Solides, Faculté des Sciences Mirande, BP138, 21004 Dijon Cedex, France*

Received March 4, 1986; in revised form July 14, 1986

The nature of the lattice disorder generated by prereactional phenomena in $Ca(OH)_2$ is investigated by single-crystal neutron diffraction. A contraction of the layers is observed and the resulting distortions along the **c** axis increase; above a critical concentration of defects, the distortions along the **c** axis can no longer increase and a disorientation of the layers occurs to accomodate the newly created defects. This disorientation causes the relaxation of the distortions. The characteristic temperatures at which the above mentioned phenomena occur are strongly dependent on the water pressure and take place far below the temperature of onset dehydration. 

## Introduction

Previous neutron and X-ray diffraction studies of the $Ca(OD)_2$ structure on polycrystalline samples revealed that prereactional transformations take place inside the material at approximately 50°C below the temperature of onset dehydration (*1, 2*). In particular, a strain relaxation occurs in the (001) planes and an abnormal increase of the deuterium thermal parameters was observed. However, this latter result had to be considered cautiously as it was based on powder data collected over a rather limited range of sin $\theta/\lambda$ and including only a small number of Bragg reflections.

This observation combined with the results of optical spectroscopy and proton conductivity obtained by Freund (*3–5*) has led us to undertake a series of single-crystal neutron-diffraction experiments aimed at obtaining more accurate values of the thermal parameters and a better understanding of the formation of the $H_2O$ molecules before their elimination from the hydroxide structure.

## Experimental

*Crystal data.* $Ca(OH)_2$ crystallizes in the hexagonal space group "$P\bar{3}m1$ ("International Tables of Crystallography," n° 164). There is one formula unit per unit cell (Fig. 1). The Ca atoms lie in the invariant positions (0, 0, 0) while the O and H atoms are located in the special positions $\pm(\frac{1}{3}\ \frac{2}{3}\ z_O)$ and $\pm(\frac{1}{3}\ \frac{2}{3}\ z_H)$.

The lattice parameters and atomic coordinates $z_O$ and $z_H$ given by different authors are reported in Table I.

* To whom correspondence should be addressed.



0022-4596/87 $3.00

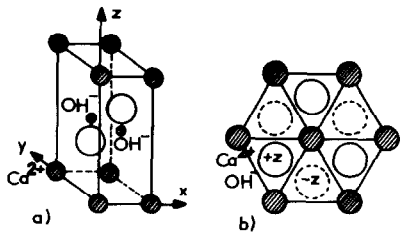


FIG. 1. The crystal structure of $Ca(OH)_2$: (a) one unit cell of the hexagonal lattice; (b) projection of three neighboring unit cells on the (00.1) plane.

*Sample.* $Ca(OH)_2$ single crystals were prepared under vacuum according to the method of Ashton and Wilson (*12*) by slow diffusion of a calcium chloride solution into a sodium hydroxide solution. They are transparent hexagonal prisms (axis of the prism = **c**) with sizes up to 1 or 2 mm.

A well shaped crystal with approximate dimensions 1.9 × 1.7 × 1.7 $mm^3$ was selected for the neutron experiment.

*Experimental procedure.* Neutron diffraction measurements were performed on the four-circle diffractometer D9 situated at the hot neutron source of the high-flux reactor of the Institut Laue-Langevin, Grenoble.

The wavelength of neutrons was 0.5467 Å. This value is based on the room temperature lattice parameters of $Ca(OH)_2$ $a$ = 3.5918 Å and $c$ = 4.9063 Å quoted by Busing and Levy (*6*).

The $Ca(OH)_2$ single crystal was held by fused silica wool in a small cylindrical Al container mounted on top of an aluminium pin. A furnace designed for the four-circle geometry (*13*) was used. It is worth noting that the actual sample temperature was lower than the measured temperature since the chromel-alumel thermocouple was fixed at the bottom of the sample-holder (i.e., a few millimeters from the sample).

In chronological order, the following sets of data were collected:

First, under vacuum ($10^{-4}$ Torr), eight sets of data between room temperature and 220°C.

Second, two other sets of data at 50 and 180°C, the crystal still being held under vacuum.

Finally, a small water vapor pressure (1.9 Torr) was introduced in the sample cell and four new sets of data were measured every 40° between 180 and 300°C.

*Data analysis.* Integrated intensities

TABLE I

STRUCTURAL DATA FOR $Ca(OH)_2$ AS REPORTED IN THE LITERATURE (RT)

| References | Techniques | $a$ (Å) | $c$ (Å) | $z_O$ | $z_H$ |
|---|---|---|---|---|---|
| Busing and Levy (*6*) | Neutron diffraction | 3.5918 (±0.0003) | 4.9063 (±0.0007) | 0.2341 (±0.0003) | 0.4248 (±0.0006) |
| Petch (*7*) | X-ray diffraction | (*8*) 3.5925 (±0.0007) | (*8*) 4.905 (±0.003) | 0.2330 (±0.0004) | 0.395 (±0.008) |
| Swanson and Tatge (*9*) | X-ray diffraction | 3.593 | 4.909 | | |
| Bernal and Megaw (*10*) | Model based on electrostatic and symmetry considerations | | | | $0.500 > z_H > z_O$ (*7*) |
| Henderson and Gutowski (*11*) | NMR | | | | 0.418 |

TABLE II

$Ca(OH)_2$ CRYSTAL STRUCTURE REFINEMENT PARAMETERS[a]

| Temperature (°C) | 20 | 50 | 80 | 110 | 140 | 174 | 199 | 220 | 50[b] | 180 | 180[c] | 220 | 260 | 300 |
|---|---|---|---|---|---|---|---|---|---|---|---|---|---|---|
| $N$[d] | 103 | 104 | 103 | 105 | 103 | 103 | 95 | 103 | 58 | 58 | 58 | 58 | 58 | 58 |
| $R$ | 0.038 | 0.037 | 0.040 | 0.043 | 0.042 | 0.043 | 0.042 | 0.043 | 0.027 | 0.033 | 0.035 | 0.036 | 0.033 | 0.038 |
| $R_w$ | 0.027 | 0.026 | 0.027 | 0.028 | 0.027 | 0.031 | 0.028 | 0.028 | 0.017 | 0.021 | 0.022 | 0.021 | 0.018 | 0.017 |
| Mosaic spread (AU) | | | | | | | | | | | | | | |
| $\perp \mathbf{c}$ | 563 | 659 | 819 | 784 | 814 | 836 | 1281 | 1550 | 1911 | 2161 | 2456 | 2330 | 3285 | 5009 |
| $\parallel \mathbf{c}$ | 188 | 183 | 196 | 207 | 173 | 157 | 133 | 132 | 130 | 124 | 124 | 114 | 165 | 215 |

[a] All data were collected on the same crystal; parameters are given in chronological order from left to right. The discrepancy indices $R$ and $R_w$ have their usual definition.
[b] Recorded after cooling from 220 to 50°C.
[c] This measurement and the next ones were recorded under a small water vapor pressure (1.9 torr).
[d] Number of independent reflections used in the refinement.

were evaluated by the $\sigma(I)/I$ criteria (*14*) and corrected for Lorentz and absorption effect. Least-squares refinement of the structure was carried out with the crystallographic program system Prometheus (*15*). The neutron scattering lengths were taken equal to 4.90, 5.805, and −3.7409 fm for Ca, O, and H atoms, respectively (*16*). All the atoms were allowed to vibrate anisotropically. The first cycles of the refinement based on unaveraged $F_{obs}$ values (with $h \geq 0$) were used to evaluate the extinction parameters. Indeed, all data, and especially those collected near room temperature, were found to be strongly affected by extinction. This was actually to be expected for these rather perfect crystals grown slowly under carefully controlled conditions. The largest effect, by far, was observed for 00$l$ reflections, which implies an anisotropic distribution of mosaic spread. As a consequence, all sets of data had to be corrected for extinction before they could be used in a structure refinement. This extinction correction was calculated in the formalism of Becker and Coppens (*17, 18*). Various extinction models were tested. The best results were obtained by assuming a Lorentzian anisotropic mosaic distribution (type I extinction). Owing to the symmetry of the lattice, only two extinction parameters were required. Refinement of these two extinction parameters decreased the discrepancy index $R_w$ from 0.063 to 0.027 (room temperature data). For sake of convenience in the following discussion, the extinction quantities $Z_{ij}$ were transformed to the equivalent mosaic spread parameters (*24*). However, it is difficult to assign any physical significance to the *absolute* values of these parameters; in the following we will therefore quote mosaic spread parameters in arbitrary units and discuss only their evolution, on a relative scale, as a function of temperature and history of the sample. Corrected intensities were then averaged and used for the final refinement of the scale factor and eight positional and thermal parameters. The number of independent reflections, $R$ factors, and extinction parameters are given in Table II.

## Results

### (*1*) *Extinction Parameters*

The temperature variation of the mosaic spread calculated from the anisotropic extinction parameters is plotted in Fig. 2: at room temperature the mosaic spread along

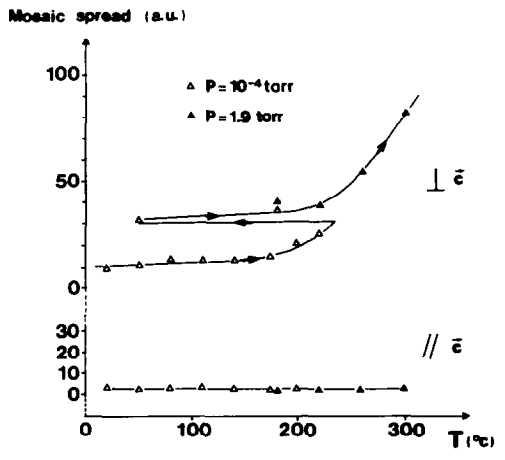


FIG. 2. Temperature variation of the mosaic spread in $Ca(OH)_2$ along and perpendicular to the c axis.

the c direction is much smaller than in the (001) planes and appears to be unaffected by the increase of temperature. In the (001) planes, the disorientations increase smoothly up to 180°C (sample under vacuum), then much faster above this temperature. This increase is found to be irreversible when the sample is cooled from 220°C back to 50°C. Renewed heating seems to cause the mosaic spread increase to amplify at approximately the same temperature even under a small water vapor pressure.

### (2) *Structural Parameters*

The final positional and anisotropic thermal parameters are listed in Table III as a function of temperature; the cell parameters and interatomic distances are given in Table IV.

*Thermal motion of the atoms.* To better visualize the atomic thermal motions, the root mean square displacements $\langle u_{\parallel}^2 \rangle^{1/2}$ and $\langle u_{\perp}^2 \rangle^{1/2}$ of each atom are plotted on Fig. 3 versus temperature. These RMS displace-

TABLE III

TEMPERATURE VARIATION OF THE POSITIONAL AND ANISOTROPIC THERMAL PARAMETERS IN $Ca(OH)_2$[a]

| Temperature (°C) | 20 | 50 | 80 | 110 | 140 | 174 | 199 | 220 | 50[b] | 180 | 180[c] | 220 | 260 | 300 |
|---|---|---|---|---|---|---|---|---|---|---|---|---|---|---|
| $z_O$ | 2340 | 2338 | 2341 | 2340 | 2340 | 2337 | 2332 | 2332 | 2343 | 2342 | 2339 | 2331 | 2329 | 2323 |
| | 3 | 3 | 3 | 3 | 3 | 4 | 4 | 4 | 3 | 5 | 5 | 5 | 5 | 5 |
| $z_H$ | 4256 | 4253 | 4250 | 4252 | 4242 | 4226 | 4212 | 4194 | 4242 | 4198 | 4206 | 4198 | 4179 | 4154 |
| | 6 | 6 | 7 | 7 | 7 | 9 | 8 | 9 | 8 | 13 | 13 | 14 | 13 | 11 |
| $U_{11}$(Å²) | 83 | 86 | 86 | 95 | 104 | 109 | 109 | 126 | 76 | 114 | 107 | 122 | 141 | 159 |
| | 4 | 4 | 5 | 5 | 5 | 6 | 6 | 6 | 6 | 8 | 8 | 8 | 7 | 7 |
| Ca | | | | | | | | | | | | | | |
| $U_{33}$ | 193 | 206 | 222 | 226 | 270 | 315 | 328 | 353 | 243 | 344 | 336 | 381 | 393 | 457 |
| | 13 | 13 | 15 | 17 | 18 | 22 | 20 | 23 | 22 | 34 | 36 | 38 | 33 | 26 |
| $U_{11}$ | 106 | 112 | 119 | 128 | 141 | 155 | 163 | 181 | 106 | 159 | 151 | 175 | 194 | 223 |
| | 3 | 3 | 3 | 4 | 4 | 4 | 4 | 4 | 4 | 6 | 6 | 6 | 5 | 5 |
| O | | | | | | | | | | | | | | |
| $U_{33}$ | 149 | 158 | 161 | 173 | 185 | 212 | 224 | 256 | 129 | 208 | 186 | 218 | 268 | 301 |
| | 6 | 6 | 7 | 8 | 8 | 9 | 8 | 10 | 11 | 16 | 16 | 16 | 15 | 13 |
| $U_{11}$ | 528 | 568 | 589 | 609 | 653 | 668 | 741 | 799 | 559 | 719 | 724 | 796 | 832 | 892 |
| | 10 | 10 | 12 | 13 | 13 | 15 | 17 | 18 | 11 | 18 | 19 | 20 | 18 | 19 |
| H | | | | | | | | | | | | | | |
| $U_{33}$ | 205 | 208 | 216 | 228 | 255 | 291 | 306 | 311 | 238 | 339 | 301 | 317 | 353 | 397 |
| | 16 | 17 | 18 | 21 | 22 | 27 | 26 | 28 | 28 | 42 | 43 | 43 | 39 | 34 |

[a] Esd's are given in the second line and refer to the last digit. Both positional and thermal parameters are multiplied by $10^4$.

[b] As in Table II.

[c] As in Table II.

TABLE IV

TEMPERATURE VARIATION OF LATTICE PARAMETERS AND INTERATOMIC DISTANCES IN $Ca(OH)_2$

| Temperature (°C) | 20 | 50 | 80 | 110 | 140 | 174 | 199 | 220 | 50[a] | 180 | 180[b] | 220 | 260 | 300 | Averaged standard deviation |
|---|---|---|---|---|---|---|---|---|---|---|---|---|---|---|---|
| $a$ (Å) | 3.5918[c] | 3.5862 | 3.5956 | 3.5993 | 3.5979 | 3.5979 | 3.6008 | 3.6074 | 3.5966 | 3.5975 | 3.6011 | 3.6041 | 3.6075 | 3.6092 | 0.0066 |
| $c$ (Å) | 4.9063[c] | 4.9010 | 4.9280 | 4.9367 | 4.9363 | 4.9399 | 4.9563 | 4.9689 | 4.9278 | 4.9518 | 4.9504 | 4.9620 | 4.9797 | 4.9837 | 0.0096 |
| Ca–O (Å) | 2.370 | 2.367 | 2.375 | 2.378 | 2.377 | 2.377 | 2.379 | 2.384 | 2.376 | 2.379 | 2.380 | 2.381 | 2.384 | 2.384 | 0.001 |
| O–O (Å) | 3.334 | 3.331 | 3.343 | 3.349 | 3.348 | 3.352 | 3.364 | 3.371 | 3.342 | 3.353 | 3.356 | 3.368 | 3.379 | 3.386 | 0.002 |
| H–H (Å) | 2.198 | 2.196 | 2.203 | 2.205 | 2.208 | 2.213 | 2.221 | 2.231 | 2.206 | 2.223 | 2.222 | 2.228 | 2.238 | 2.248 | 0.002 |
| O–H (Å) | 0.940 | 0.938 | 0.941 | 0.943 | 0.939 | 0.933 | 0.932 | 0.925 | 0.936 | 0.919 | 0.924 | 0.926 | 0.921 | 0.912 | 0.005 |
| $O-H_{corr.}$[d] (Å) | 0.987 | 0.988 | 0.992 | 0.995 | 0.995 | 0.989 | 0.995 | 0.993 | 0.985 | 0.981 | 0.988 | 0.994 | 0.992 | 0.987 | |

[a] As *b* in Table II.
[b] As *c* in Table II.
[c] These lattice parameters were used to calibrate the wavelength.
[d] Corrected for proton thermal motion.

ments are relative to the motion of the atoms about their equilibrium position parallel and perpendicular to the **c** axis, respectively. The anisotropy is very large for the Ca and H displacements but rather small for the oxygens, as already reported by Busing and Levy for the room temperature structure (*6*). The largest thermal motion of the H atoms occurs perpendicular to the O–H bond; this led Busing and Levy to suggest that the protons in $Ca(OH)_2$ undergo an "umbrella"-type vibration subtending a cone of angle $\alpha$ with respect to the **c** direction. Therefore, the O–H bond length has to be corrected of this "umbrella"-type vibration (Table IV).

*Thermal expansion of the atomic layers.* The layer structure of $Ca(OH)_2$ along the **c** direction is schematically depicted in Fig. 4.

Let $e_1$, $e_2$, $e_3$ be the distances between the atomic planes containing Ca and O, O and H, H and H, respectively. Let $e_2'$ and $e_3'$ be the distances O–H and H–H corrected of the "umbrella" motion of the H atoms.

All the interlayer distances defined above are plotted on Fig. 5 as a function of temperature. $e_1$ increases slightly with temperature up to 300°C as do $e_2$ and $e_3$ until about 130°C. Above 130°C, a change of slope occurs in the latter two curves: $e_2$ starts to decrease while $e_3$ increases rapidly. These effects, although reduced, are still observed after correction of the proton motion around the O atoms ($e_2'$, $e_3'$).

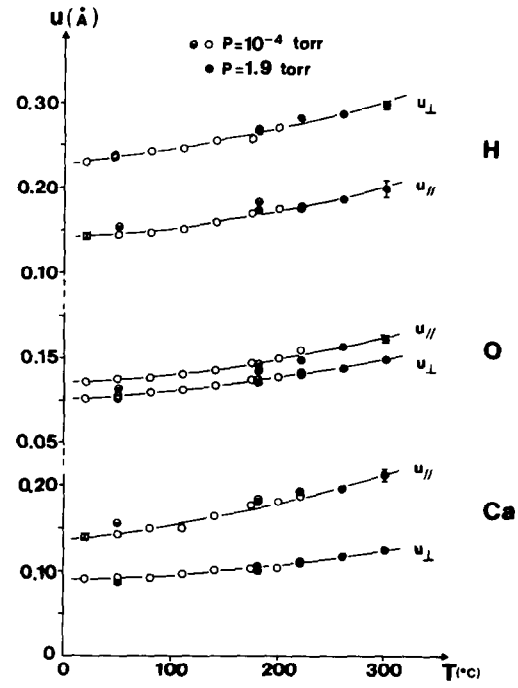


FIG. 3. Root mean square displacements $u_{\parallel}$ and $u_{\perp}$ of Ca, O, and H atoms along and perpendicular to the **c** axis as a function of temperature. The line is only a guide to the eye. Open circles, first heating; half-full circles, second heating (vacuum); full circles, second heating (under vapor pressure). Error bars correspond to 2 esd.

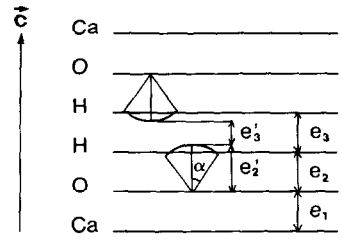


FIG. 4. Schematic drawing of the layered structure of $Ca(OH)_2$.

## Discussion

The room temperature positional and thermal parameters obtained in the present study are in good agreement with previous results by Busing and Levy (see Table V).

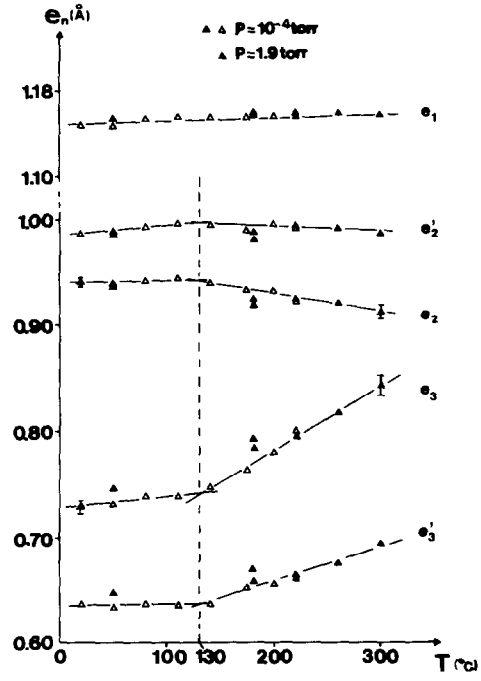


FIG. 5. Temperature evolution of intralayer distances along the c axis in $Ca(OH)_2$. $e_1$, $e_2$, $e_3$ = Ca–O, O–H, H–H distances, resp. $e'_2$, $e'_3 = e_2$ and $e_3$ but corrected for the thermal motion of the H atoms perpendicular to the O–H bond. Notation as in Fig. 3.

Their temperature evolution together with the concomitant variation of the mosaic spread shed some light on the prereactional transformations which take place inside the solid well below the onset of the dehydration.

### *1. Characterization of the Lattice Disorder in $Ca(OH)_2$ at Room Temperature*

The anisotropy of the mosaic spread gives evidence of a domain misorientation much larger perpendicular to than along the c axis. These results allow a better characterization of the lattice defects shown by earlier diffraction studies on powder samples (*1*). Indeed, from an analysis of the powder diffraction line broadening, it can be shown that strong lattice distortions take place in the stacking of the hexagonal layers or, more precisely, that there is a distribution of $d_{001}$ spacings. Possible causes of this fluctuation may be either a puckering of the layers (Fig. 6a) or nonequidistance of the layers, including or not a misorientation of the c axis (Figs. 6b, c). The narrow mo-

TABLE V

STRUCTURAL PARAMETERS OF $Ca(OH)_2$ ($T$ = 20°C)

| | | Busing and Levy (*6*) | This work |
|---|---|---|---|
| $z_O$ | | 0.2341 (3) | 0.2340 (3) |
| $z_H$ | | 0.4248 (6) | 0.4256 (6) |
| Ca | $U_\perp$[a] (Å) | 0.094[b] | 0.0909 |
| | $U_\parallel$ | 0.125 | 0.1388 |
| O | $U_\perp$ | 0.096 | 0.1029 |
| | $U_\parallel$ | 0.109 | 0.1220 |
| H | $U_\perp$ | 0.231 | 0.2298 |
| | $U_\parallel$ | 0.130 | 0.1433 |
| O–H (Å) | | 0.936 (3) | 0.940 (3) |
| O–$H_{corr.}$[c] | | 0.984 (4) | 0.987 |

[a] $u_\perp$ and $u_\parallel$ denote the RMS displacements $\perp$ and $\parallel$ to the c axis, resp., as defined in the text.

[b] These RMS displacements were calculated from the $B$ temperature factors given by Busing and Levy.

[c] Corrected for proton thermal motion.

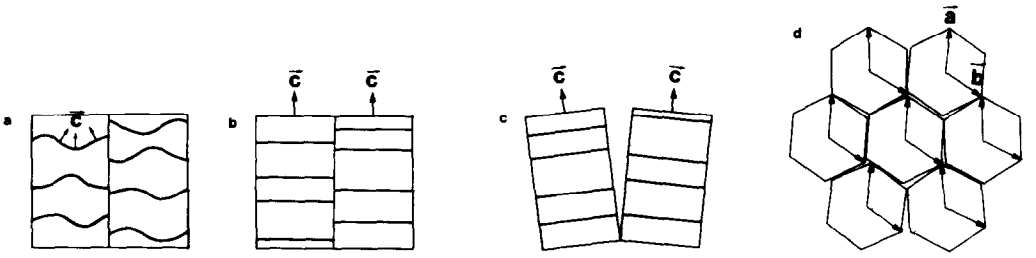


FIG. 6. Schematic representation of the layers in the $Ca(OH)_2$ structure (a–c) along and (d) perpendicular to the **c** axis.

saic spread of the **c** axis rules out the puckered layer explanation and leaves as the only possibility unequal spacing of planes along **c** (Fig. 6b). On the other hand, we also found from the analysis of the powder data (*1*) that the distortions are minimum in the directions perpendicular to the **c** axis which gives evidence for a narrow distribution of $d_{hk0}$ spacings. In addition, the large orientation distribution of the **a** axis as measured from single-crystal data indicates that the coherently scattering domains in the (001) planes are slightly rotated with respect to each other around the **c** axis (Fig. 6d).

To summarize these results one can say that the lattice disorder occurring above $T_1$ (Fig. 7) is such that the domains scattering coherently remain well oriented with respect to the **c** direction but that the interplanar spacing along this direction is not constant while large misorientations develop perpendicular to the **c** axis but without any variation in the spacing of *hk*0 planes.

### 2. *Temperature Evolution of the $Ca(OH)_2$ Structure*

Some changes occur in the hydroxide layers with increasing temperatures. They show up as a sudden increase of the mosaic spread in the (001) planes above about 180°C (Fig. 2) and by a discontinuity of the thermal expansion of the distances O–H and H–H at about 130°C (Fig. 5).

(*A*) *Lattice disorder.* With the powder sample, a sudden decrease of the lattice distortions in the **c** direction was observed at 130°C (true sample temperature) under vacuum (*1*). However, we noticed that both the defect relaxation and the decomposition

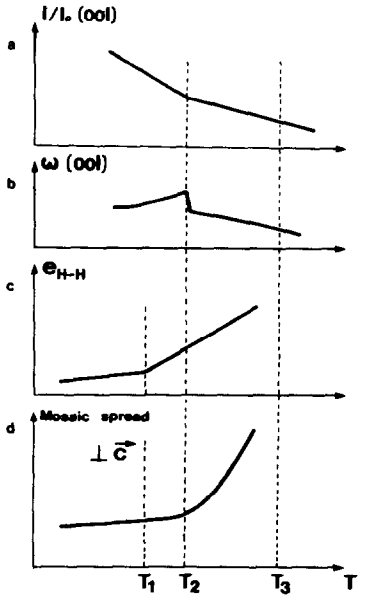


FIG. 7. Diagrammatic temperature correspondence between the various prereactional phenomena detected by diffraction studies during a thermal treatment of $Ca(OH)_2$: Intensity (a) and width (b) of the 00*l* lines as shown by powder diffraction (Fig. 6 and Fig. 1 in Ref. (*1*)). Interlayer H–H distance (c) and mosaic spread (d) as measured by single-crystal diffraction (Fig. 5 and Fig. 2 in this study). $T_1$, $T_2$, $T_3$ are defined and discussed in the text.

reaction were shifted to higher temperatures by a slight increase of the water vapor pressure in the reaction cell. It was therefore suggested that the defects and their evolution may be controlled by a chemical and structural transformation which occurs in the solid long before the onset of the decomposition reaction. The sudden increase of mosaic spread also takes place in the crystal long before the onset of the dehydration. Therefore, it is reasonable to associate it also with this prereactional transformation. It is worth mentioning that the crystal remained transparent after the experiment: this is a proof that no water has evolved from the crystal and that no local hydroxide into oxide phase change took place.

The comparison between the characteristic temperatures observed on powder and single-crystal experiments unfortunately is made difficult by the large differences of experimental set up. Indeed, in the case of powder experiments, the temperature could be measured accurately by a thermocouple placed inside the sample and the residual vapor pressure precisely monitored. This is no longer true for the crystal experiment: the distance between the thermocouple and the sample in an evacuated cell implies an overestimation of the true sample temperature. In addition the constraints of the four-circle geometry do not allow a precise measurement of the residual vapor pressure in the sample cell; however, it is reasonable to assume that the vapor pressure is higher than $10^{-4}$ torr and this gives rise to a shift of the characteristic temperatures toward higher temperatures (see Fig. 1 and Fig. 4 of Ref. (*1*)).

Therefore, it is rational to assume that the relaxation of the distortions and the mosaic spread increase occur simultaneously (temperature $T_2$ in Fig. 7).

(*B*) *Interatomic distances*. The temperature dependence of the characteristic distances of the structure is represented in Fig. 5. The Ca–O distance is almost temperature independent in the range RT–300°C; this was to be expected from the strength of the Ca–O bond and means that the thermal expansivity of the inner part (O–Ca–O) of the layers is almost negligible. The most prominent features are the increase of the interlayer H–H distance ($e_3$) and the concomitant contraction of the O–H bond ($e_2$) above about 130°C (Fig. 5).

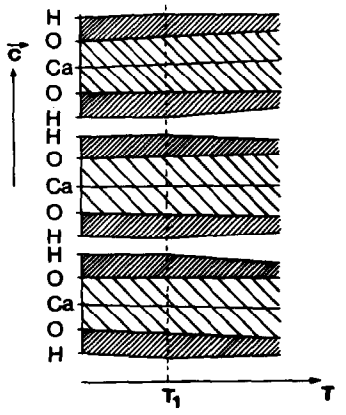


FIG. 8. Schematic drawing of the temperature evolution of the inter- and intralayer distances in $Ca(OH)_2$.

### *3. Sequence of Pretransitional Effects before $Ca(OH)_2$ Dehydration*

The phenomena which take place in the crystal well below the decomposition of $Ca(OH)_2$ into CaO can tentatively be summarized in the following way by introducing three characteristic temperatures (Fig. 7):

Below $T_1$, regular behavior (normal thermal expansion).

Between $T_1$ and $T_2$ protons start to delocalize as evidenced by the shrinkage of the layers (Fig. 8). The resulting distortions lead to a broadening of the 00*l* lines in the powder diffraction pattern (Fig. 1 in Ref.

(*1*) and Fig. 7b in present work) and to a steep variation of their intensities (Fig. 6 in Ref. (*1*) and Fig. 7a in present work) due to the existence of an additional contribution to the thermal parameters (static Debye-Waller).

Above a critical concentration of defects which occur at $T_2$, the lattice can no longer cope with additional defects by increasing the distortions along the **c** axis; it is now the disorientation of the layers with respect to each other which allows to accomodate the newly created defects and therefore the relaxation of the distortions.

Above $T_3$, decomposition into CaO takes place and leads to the destruction of the crystals.

The characteristic temperatures $T_1$, $T_2$, $T_3$ are strongly dependent on the physicochemical parameters of the sample environment and especially the residual water vapor pressure $P$:

The evolution of $T_3$ as a function of $P$ has been extensively studied in previous work (*19–21*). In our powder experiments (*1*) we found, for instance, $T_3 = 215°C$ with $P = 10^{-4}$ Torr and $T_3 = 307°C$ with $P = 1.8$ Torr.

In the same powder experiments $T_2$ was found at 115°C ($P = 10^{-5}$ Torr) (*22*), 130°C ($P = 10^{-4}$ Torr, Fig. 1 and Fig. 2 in Ref. (*1*)), and 170°C ($P = 1.8$ Torr, Fig. 4 and Fig. 5 in Ref. (*1*)). In the single-crystal experiment $T_2 \simeq 180°C$; $P$ could not be measured but is estimated to be much higher than $10^{-4}$ Torr.

$T_1$ was only determined in the single-crystal experiment ($T_1 \simeq 130°C$). It should show up in powder diffraction experiments as an increase of the line breadth; however, this is probably a rather weak effect and it was not observed due to the limited accuracy of the measurements (*1*). Nevertheless, it is worth noting that a recent NMR study (*23*), in agreement with the work of Freund (*3–5*) gave evidence of mobile protons in the hydroxide structure and an additional proton motion was found to occur above about 60°C. This temperature may be identified with the temperature $T_1$ mentioned in the present study. However, these authors conclude that above this temperature most of the protons are highly mobile; this conflicts with the results of the present work which do not show any anomaly in the evolution of the thermal parameters in the range RT–300°C.

## Conclusion

This study was undertaken to obtain more accurate values of the thermal parameters and a better understanding of the formation of the $H_2O$ molecules before their evolution from the hydroxide structure. At variance from the previous powder-diffraction results, it does not indicate any abnormal variation of the thermal parameters of the H atoms and therefore do not bring direct information on the mecanism of formation of the $H_2O$ molecules in the solid before the dehydration. However, the temperature evolution of the mosaic spread and of the interlayer and interatomic distances give evidence of prereactional transformations, i.e., of changes occuring inside the initial crystal long before any loss of water and long before the beginning of transformation of the hydroxide structure into the oxide structure.

Finally, the determination of the mosaic spread in the crystal provided additional informations about the nature of the lattice disorder in the $Ca(OH)_2$ structure and about its variation with temperature.

## Acknowledgment

We thank Dr. P. J. Brown for a critical reading of the manuscript.

## References


1. O. CHAIX-PLUCHERY, J. BOUILLOT, D. CIOSMAK, J. C. NIEPCE, AND F. FREUND, *J. Solid State Chem.* **50,** 247 (1983).
2. O. PLUCHERY, Thèse de 3ème Cycle, Université de Dijon, 1982.
3. F. FREUND AND H. WENGELER, *Ber. Bunsenges. Phys. Chem.* **84,** 866 (1980).
4. H. WENGELER, R. MARTENS, AND F. FREUND, *Ber. Bunsenges. Phys. Chem.* **84,** 873 (1980).
5. F. FREUND, H. WENGELER, AND R. MARTENS, *J. de Chimie Physique* **77,** 837 (1980).
6. W. R. BUSING AND H. A. LEVY, *J. Chem. Phys.* **26,** 563 (1957).
7. H. E. PETCH, *Acta Crystallogr.* **14,** 950 (1961).
8. H. D. MEGAW, *Proc. R. Soc. London Ser. A.* **142,** 198 (1933).
9. SWANSON AND TATGE, *Nat. Bur. Stand. Circ. 539* **1,** 58 (1953).
10. J. D. BERNAL AND H. D. MEGAW, *Proc. R. Soc. London Ser. A* **151,** 384 (1935).
11. D. M. HENDERSON AND H. S. GUTOWSKI, *Am. Mineral.* **47,** 1231 (1962).
12. F. W. ASHTON AND R. WILSON, *Am. J. Sci.* **5,** 209 (1927).
13. G. HEGER, W. F. KUHS, AND S. MASSING, *Rev. Phys. Appl.* **19,** 735 (1984).
14. M. S. LEHMANN AND F. K. LARSEN, *Acta Crystallogr. Sect. A* **30,** 580 (1974).
15. U. H. ZUCKER, E. PERENTHALER, W. F. KUHS, R. BACHMANN, AND H. SCHULZ, *J. Appl. Cryst.* **16,** 358 (1983).
16. L. KOESTER AND H. RAUCH, IAEA-Contract 2517/RB (1981).
17. P. BECKER AND P. COPPENS, *Acta Crystallogr. Sect. A* **30,** 129 (1974).
18. P. BECKER AND P. COPPENS, *Acta Crystallogr. Sect. A* **31,** 417 (1975).
19. P. E. HALSTEAD AND A. E. MOORE, *J. Chem. Soc.*, 3873 (1957).
20. P. J. WYLLIE AND O. F. TUTTLE, *J. Am. Ceram. Soc.* **42,** 448 (1959).
21. J. C. NIEPCE, unpublished work.
22. Experimental report n° 5-21-146, ILL Grenoble (1981).
23. J. A. MORENO, S. MIZRACHI, AND V. OPPELTZ, *Solid State Commun.* **51,** 597 (1984).
24. P. COPPENS AND W. C. HAMILTON, *Acta Crystallogr. Sect. A* **26,** 71 (1970).